

Development and decay of vortex flows in viscoelastic fluids between concentric cylinders

Renzo Guido, Felipe Rinderknecht, Cecilia Cabeza, Arturo C. Martí, Gustavo Sarasúa

Iguá 4225, Instituto de Física, Facultad de Ciencias, Universidad de la República,
Montevideo, Uruguay

E-mail: marti@fisica.edu.uy

Abstract. We study the development and decay of vortex in viscoelastic fluids between coaxial cylinders by means of experiments with solutions of polyacrylamide and glycerin and numerical simulations. The transient process is triggered when the inner cylinder is either abruptly started or stopped while the outer is kept fixed. The azimuthal velocity, obtained by means of digital particle velocimetry, exhibits oscillations before reaching the stationary state. The development of the vortex is characterized by means of the overshoot, i.e. the difference between the maximum and the stationary velocity. Analogously, in the decay of the vortex, the azimuthal velocity changes its direction and the relevant parameter is the undershoot defined as the maximum reversed transient velocity. To get a deeper insight into this phenomenon, the experimental results are supplemented with numerical simulations of rheological models as the Oldroyd-B and White-Metzer. The results obtained with the first model reveal the dependence of the overshoot and undershoot with the elasticity number of the fluid. Using the White-Metzer model we explain the increase of the overshoot produced by the reduction of the solvent viscosity in terms of the shear-thinning effects.

1. Introduction

Many industrial applications, as the production of food, lubricants, paints, among many others, involve the flow of non-Newtonian fluids, in general much more complex than their Newtonian counterpart [1]. Non-Newtonian flows have been studied in numerous configurations, however, one aspect that has received comparatively less attention is their transient dynamics [2, 3]. Here we consider the development and decay of vortex flows in non-Newtonian fluids [4, 5, 6]. In particular, we consider a system composed of two cylinders in which the outer is kept fixed while the inner can be abruptly put in motion or stopped. Due to the presence of the "hoop" stress in flows of viscoelastic fluids with curved streamlines [2], we expect the behavior of the transient rotational flows in such systems exhibits remarkable differences with that developed in Newtonian fluids.

Several experimental studies have been conducted to study the development and decay of vortex flow of viscoelastic fluids in cylindrical containers [7, 8, 9, 10]. However, the experimental study of the transient vortex flow in viscoelastic fluids between cylinders has received little attention. In a pioneering contribution, Groisman and Steinberg [11] reported the influence of small polymer addition on the stability and pattern selection of the Taylor-Couette flow. In contrast with the well-known Newtonian case, in the polymeric flow they found oscillatory behavior attributed to the fluid elasticity. Later, the flow of different polymer solutions between coaxial cylinders was also experimentally considered in [12], where the variation of the torque on the inner cylinder compared with the Newtonian case was obtained and showed to exhibit hysteretic behaviors.

The unsteady rotational flows of viscoelastic fluids have been theoretically studied making use of different models. Using a fractional Maxwell model, Qi and Jin [4] analyzed two unsteady flows between coaxial cylinders. In the first the outer cylinder performs a simple harmonic motion while the inner cylinder is kept still while in the second the outer cylinder suddenly starts up and rotates at a constant speed while the inner cylinder is kept stationary. In these problems the theoretical model predicted either oscillations or an initial peak followed by a relaxation to an steady value respectively in the evolution of the azimuthal velocity. Fractional calculus was proposed to obtain exact solutions using for the decay of a potential vortex in Oldroyd-B and Maxwell fluids [5, 6]. Closed expressions for the velocity components and their dependence with the model parameters and the fractional coefficients were reported in these studies.

In this work we consider two complementary transient dynamics. In the first one we explore the start up of the swirling flow from the quiescent fluid after the inner cylinder suddenly begins to rotate. In the second one, we examine the decay of the initially steady vortex flow after the inner cylinder becomes abruptly at rest. The experimental results show that, in contrast with Newtonian flows, the azimuthal velocity reaches a maximum before decaying in the case of the development of a vortex, while it changes

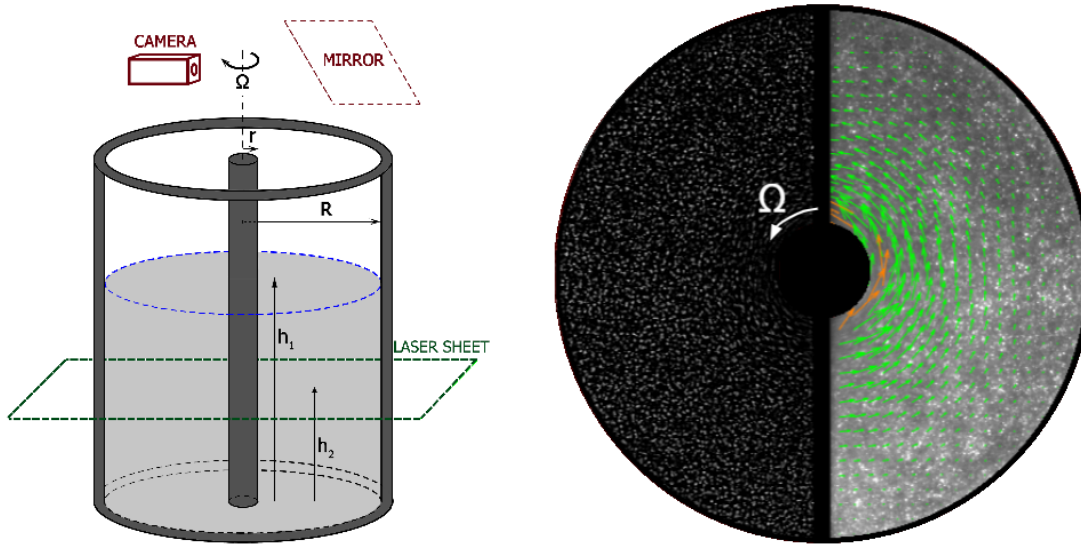


Figure 1. Panel (a) schematizes the experimental set up. The cylinders are shown in solid lines, with radius R and r . The laser plane is indicated at a height h_2 with a dash line, and the fluid’s surface is at height h_1 . The camera is 1.5 m from the axis and points to the mirror above the cylinders. Panel (b) is a example of a picture taken from the video (left) and its DPIV (right). The height of the plane is 45 mm . The camera only recorded a half of the circle, so the picture on the left was mirrored.

its direction in the case of the decay. These behaviors can be characterized by two dimensionless parameters, denoted overshoot and undershoot. In order to get a deeper insight into this phenomenon we carried out numerical simulations using the Oldroyd-B and White-Metzer (WM) models. These simulations allow to identify the elasticity of the fluid and the shear-thinning effects as being related to this peculiar transient behavior. The rest of this article is organized as follows. In section 2 we describe the experimental setup, the methodology and the working fluids. In section 3 we present the experimental results. The numerical results described in Section 4 generalize the experimental results. Finally, Section 5 presents the discussion and conclusion.

2. Experimental setup

The core of the experimental setup schematized in Fig. 1 consists of two concentric acrylic cylinders. The external of radius $R = 41.65 \pm 0.05\text{ mm}$ is kept fixed, and the internal whose radius is $r = 4.75 \pm 0.05\text{ mm}$ is able to rotate driven by a direct current motor. Its maximum angular velocity is $\Omega = 7.0\text{ rad/s}$. The height of the fluid column is $h_1 = 100 \pm 1\text{ mm}$. The bottom is fixed and the fluid upper surface is free at atmospheric pressure.

The fluids used in this experiment were four shear-thinning solutions of Polycarylamide (92560-50G Sigma-Aldrich) in mixtures of water and glycerin enumerated in Table 1. The rheological properties of the different fluids were measured at 20°C , with an Anton Paar Physica MCR 301 rheometer. For each fluid, the

Properties	P1G30	P1G60	P2G30	P2G60
Glycerin (%)	30	60	30	60
Polyacrylamide (%)	1.0	1.0	2.0	2.0
μ_0 (Pa·s)	4.65	4.40	107	157
ν_0 ($\times 10^{-3}$ m ² /s)	4.39	3.93	101	140
λ (s)	9.8	2.2	42	46
Re($\times 10^{-3}$)	29.0	32.5	0.91	1.26
De	55.4	12.4	237	260
E($\times 10^3$)	1.91	0.383	188	286

Table 1. Fluid samples used along the experiments and their rheological properties. The rotational velocity used for calculating the Reynolds and Deborah number was 5.65 rad/s.

strain dependent dynamics viscosity, $\eta(\dot{\gamma})$, was fitted to the Carreau model $\eta(\dot{\gamma}) = \eta_0(1 + (\lambda\dot{\gamma})^2)^{(n-1)/2}$ to obtain the viscosity at zero-shear rate, η_0 , and the characteristic time, λ , as shown in this table.

The relevant dimensionless parameters to characterize the viscoelastic effects are the Deborah and elasticity numbers. The Deborah number is defined as $De = \lambda U/R$, where R is the radius of the inner cylinder, U is the velocity at the surface of that cylinder and λ is the characteristic time. The elasticity number is defined as $E = De/Re$, where $Re = UR/\nu_0$ is the Reynolds number and ν_0 the zero-shear kinematic viscosity. Using the angular velocity of the inner cylinder Ω , these numbers can be written as $De = \lambda\Omega$, $Re = \Omega R^2/\nu_0$ and $E = \lambda\nu_0/R^2$. The specific values for each fluid, which are independent on Ω , are listed in Table 1.

The velocity fields were measured by means of Digital Particle Imaging Velocimetry (DPIV), which is based on 2D cross-correlation of consecutive images. To this end, the fluid was seeded with neutrally buoyant nearly-spherical polyamide particles (Dantec Dynamics, Denmark). The particles with mean diameter of 50 μm and Stokes number of approximately 10^{-4} can be assumed to closely follow the flow. The particles were illuminated in the horizontal plane shown in the figure at height $h_2=45$ mm from the bottom. A green laser LaserGlow (model LSR-0532-PFH-005500-05n) was used for this purpose. The light reflected by the particles was captured by a Pixelink (model PL-B7760) digital camera using a mirror at 45° fixed above the cylinders and working 45 fps. As the velocity in the region close to the external cylinder is small, the DPIV was performed averaging three consecutive frames. Then, the velocity field was obtained at a sampling frequency of 15 Hz in a Cartesian grid. At the rotation velocities involved in our experiments the velocity fields observed were almost axisymmetric. To obtain the azimuthal component each grid point was classified according to its distance to the rotation axis in rings of 2.05 mm thickness. At each time, we calculated the averaged azimuthal velocity and its standard deviation.

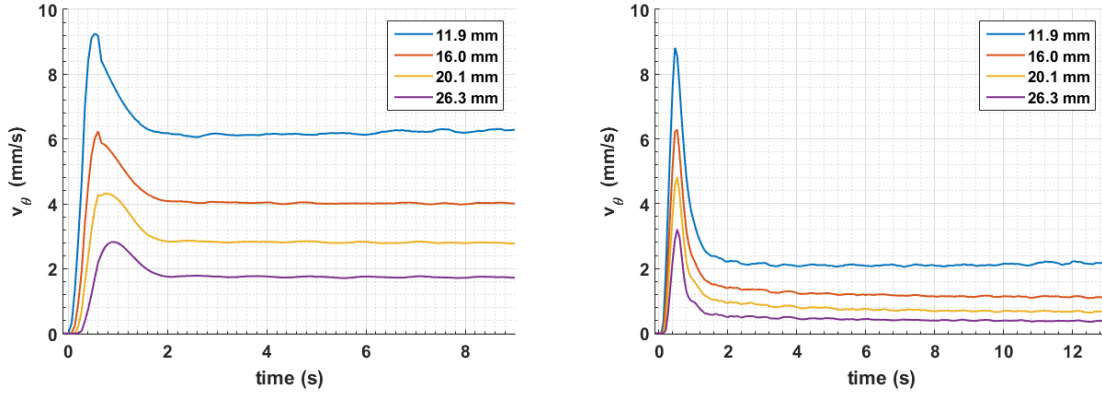


Figure 2. Temporal evolution of the azimuthal velocity at different distances to rotation center indicated in the legend boxes. Panel (a) corresponds to the fluid P1G30 and (b) to the P2G30. The initial time, $t = 0$, corresponds to the instant when the motor was turned on. The uncertainties are nearly constant and their mean values are 0.4 mm/s, 0.2 mm/s, 0.2 mm/s and 0.1 mm/s respectively for each axial distance.

3. Experimental results and analysis

3.1. Start-up of the vortex flow

In this section we describe the experiments performed to study the development of the vortex flow departing from the quiescent fluid. In these experiments the inner cylinder is initially at rest and abruptly begins to rotate with a constant angular velocity Ω . In Fig. 2 we show the temporal evolution of the azimuthal component of the velocity at different axial distances for the fluids P1G30 and P2G30. In all the cases, the azimuthal velocity reaches a maximum and then decreases approaching a stationary value. This characteristic behavior is present in all the fluids analyzed.

Inspired in control theory [13], to quantify this characteristic behavior we define the overshoot as the dimensionless parameter $M_p = (v_{max} - v_{st})/v_{st}$ where v_{max} and v_{st} are the maximum and the stationary value of the velocity.

In Fig. 3 we plot the overshoot as a function of the distance to the center of rotation, r , for all the fluids samples considered. Several relevant aspects can be noted in this figure. First, we observe that in all the cases the overshoot increases with the radial coordinate indicating a relationship with positive streamlines curvature. Nonetheless, this effect is more notorious when the polymer concentration is 2%, fluids P2G30 and P2G60, in comparison with the samples in which the concentration is 1%, P1G30 and P1G60. This results clearly suggest a positive relationship of the overshoot with the elastic modulus. In addition, when we compare fluid samples with the same polymer concentration but different glycerin concentration we note that the overshoot increases with decreasing the concentration suggesting that the viscous part of the fluid also plays an important role in this phenomenon.

After that we repeated the experiments starting again from a fluid at rest but considering different final angular velocities. In Fig. 4, corresponding to fluid sample

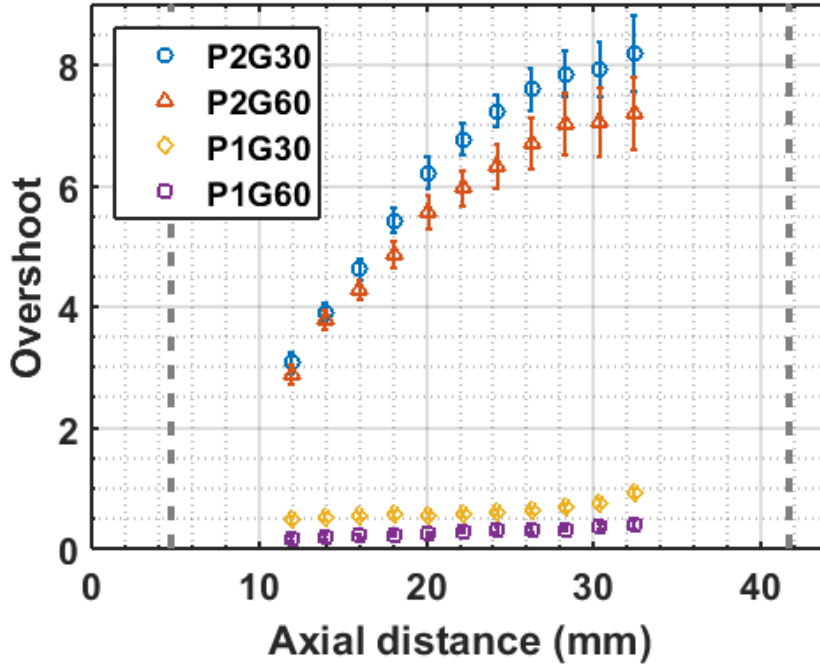


Figure 3. Overshoot increases with the axial distance for all the samples. The difference between the samples with 1% of polyacrylamide and those with 2% is enormous. The borders of the cylinders are indicated with vertical dashed lines.

P2G30, we observe the overshoot as a function of the axial distance for four different rotational velocities. We notice a dependence in which the overshoot increases with increasing the angular velocity. Nonetheless, this effect is more noticeable for the regions close to the inner cylinder.

3.2. Decaying vortex

In this section we study the decaying of the vortex flow when the inner cylinder, initially rotating at constant speed, is abruptly stopped. As shown in Fig. 5(a), corresponding to the fluid P1G30, the azimuthal velocity starts at a steady value, then it decreases quickly, reverses its direction until reaching a maximum negative (opposite) value and then decreases (in magnitude) approaching a null velocity. This behaviour is presented for all the curves in Fig. 5(a), corresponding to different distances from the cylinder's axis. The panel (b) shows the temporal evolution of the azimuthal velocity for the fluid P2G30, where the reversal of the velocities is also observed. Similar to that observed in the development of the vortex, the effect is more notorious in the P2G30 fluid than for the P1G30 in which the concentration of polyacrylamide is larger in the first than in the latter.

Similarly to the overshoot defined in the development of the vortex, it is possible to introduce a dimensionless parameter for the reversal of the fluid, referred to as

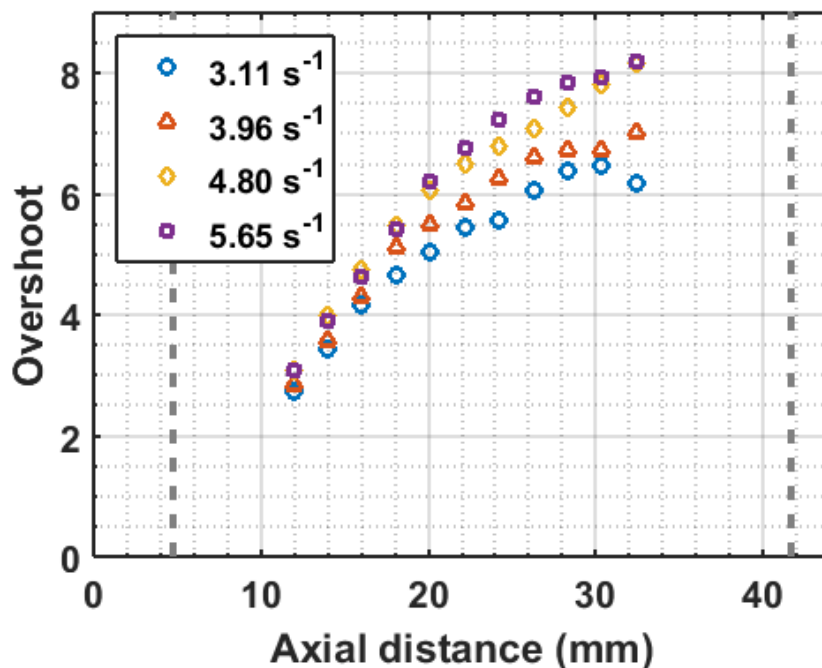


Figure 4. Overshoot as a function of axial distance for four rotational velocities indicated in the legend box. The fluid sample is the P2G30. As in the previous figure, the borders of the cylinders are indicated with vertical dashed lines.

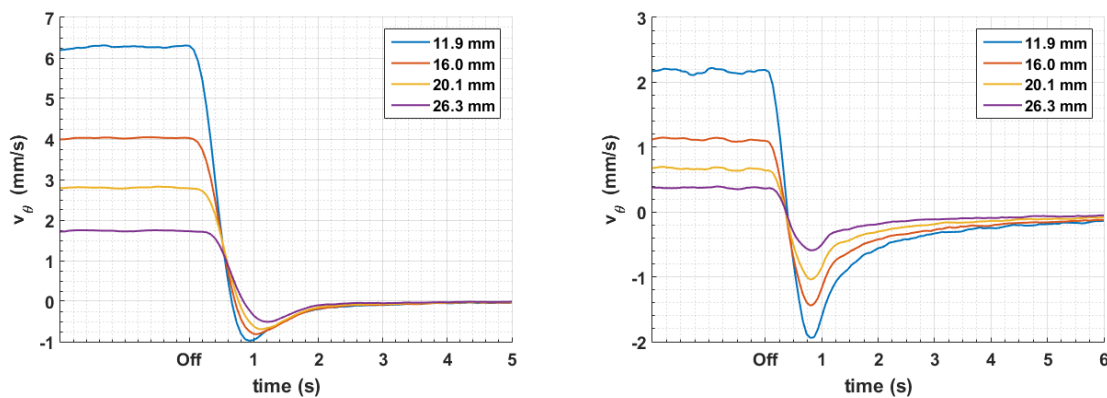


Figure 5. The undershoot is manifested in the temporal evolution of the azimuthal velocity when the inner cylinder is abruptly stopped at the time indicated in the horizontal axis. The different curves correspond to different axial distances indicated in the legend boxes. Panels (a) and (b) correspond to P1G30 and P2G30 respectively. The uncertainties in the velocities are 6%.

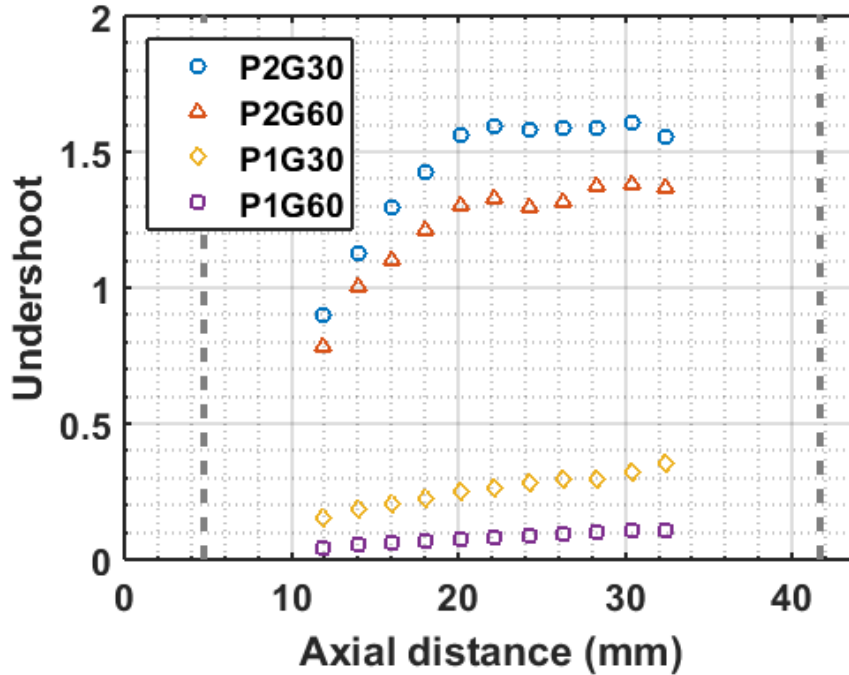


Figure 6. Undershoot as a function of axial distance for all the fluid sample. The difference observed between high and small polyacrilamide concentration is remarkable. At small elastic modulus, the undershoot increases with axial distances. Also, the smaller solvent viscosity fluid P1G30 exhibits a larger reversal. At high elastic modulus, the effect increases with axial distance until it reaches a plateau. As in the previous experiment, the samples P2G60 and P2G30 reveal similiar behaviours.

undershoot or relative maximum negative peak value [13], $M_{mn} = \left| \frac{v_{mn}}{v_{st}} \right|$ where v_{mn} is the maximum negative (or opposite) velocity. The dependence of the undershoot with the axial distance for each fluid is shown in Fig. 6 for all the fluid samples studied. It can be noticed that samples with higher elastic components exhibit notoriously larger undershoots, a qualitative behaviour similar to that reported in Fig. 3 for the overshoot. Moreover, comparing samples with the same polyacrylamide concentration and different viscosity, those with smaller viscosity exhibit a larger effect.

4. Numerical Simulations

4.1. Oldroyd-B governing equations

To get a deeper insight into the transient behavior of the vortex flows we performed numerical simulations using the well-known Oldroyd-B model [14] which can be considered as an extension of the Maxwell model and is equivalent to a fluid filled with elastic beads and spring dumbbells. Our aim was to determine the role of the elastic component of the fluid and the solvent viscosity in the overshoot and undershoot observed in the experiments reported in the previous section. According to the Oldroyd-

B model, the dimensionless governing equations of a viscoelastic incompressible fluid are given by

$$\text{Re} \frac{D\mathbf{v}}{Dt} = -\nabla p + \beta \nabla^2 \mathbf{v} + \nabla \cdot \sigma, \quad (1)$$

where σ is the polymeric stress tensor, β is the ratio between the solvent and total viscosities, $\beta = \mu_s/(\mu_s + \mu_p)$, being μ_p the polymer viscosity. The polymeric stress tensor of an Oldroyd-B model satisfies the evolution equation

$$\text{De} \left(\frac{\partial \sigma}{\partial t} + \mathbf{v} \cdot \nabla \sigma - \sigma \cdot \nabla \mathbf{v} - \nabla \mathbf{v}^\dagger \cdot \sigma \right) + \sigma = -(1 - \beta)(\nabla \mathbf{v} + \nabla \mathbf{v}^\dagger). \quad (2)$$

In the statistical derivation of the Oldroyd-B model starting from a microscopic approach it can be shown that

$$\lambda = \frac{3\pi a \mu_s}{4k_B T \beta_L^2}, \quad (3)$$

$$\mu_p = \frac{3\pi m a \mu_s}{4\beta_L^2} \quad (4)$$

where k_B is the Boltzmann constant, T the absolute temperature, m the polymer concentration, and, finally, a and β_L^{-1} are characteristic lengths of the polymeric chain model [15]. Another important parameter for our purposes is $G = \mu_p/\lambda = mk_B T$, which measures the influence of the polymeric concentration on the fluid properties.

We solved the constitutive equations, Eqs. (1-2), using the finite element computational package COMSOL [16] which has been shown to be a reliable tool in different computational fluid dynamics problems (see for example Refs. [17, 18]). The code validation has been done considering the flow of a viscoelastic fluid past a cylinder. Assuming axial symmetry, we performed simulations on two dimensional meshes in which the inner and outer cylinders are located at R and $10R$ respectively and the fluid depth is $h = 20R$. A more refined mesh was used near the inner cylinder to avoid numerical instabilities. Neglecting air viscosity and surface tension, the interface between the viscoelastic fluid and the air was simulated as an horizontal wall with a slip boundary condition. This approximation agrees very well with the experiments in which the interface only slightly deviates from the horizontal plane.

We numerically simulated the temporal evolution of the velocity field starting with a fluid at rest for three different meshes with 2^{13} , 2^{14} and 2^{15} elements. The differences between the three meshes were negligible, with a maximum difference in azimuthal velocity of 0.6 % for 2^{13} and 2^{15} elements, and 0.3 % for 2^{14} and 2^{15} elements. We defined dimensionless quantities based on the stationary angular velocity and the inner cylinder radius. In Fig. 7 the curves of dimensionless azimuthal velocity v_θ/U at the position $r = 2$, $z = 10$ are compared for different values of E . These curves reveal that according to the Oldroyd-B model the overshoot is clearly enhanced with the increment of E .

In addition, the numerical results indicate that there is always an overshoot for any finite value of λ , but its value can be strongly reduced as E is decreased. Figure 7 shows

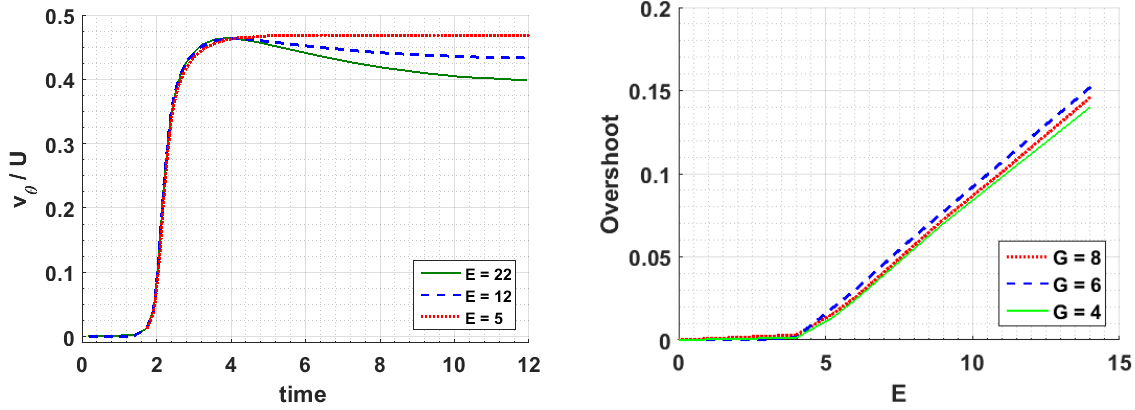


Figure 7. Panel (a) shows dimensionless azimuthal velocity as a function of time for different elasticity values, E , indicated in the legend box. Panel (b) corresponds to the overshoot parameter M_p as a function of E and different values of the parameter G which characterises the polymeric concentration indicated. In both panels $Re = 0.1$.

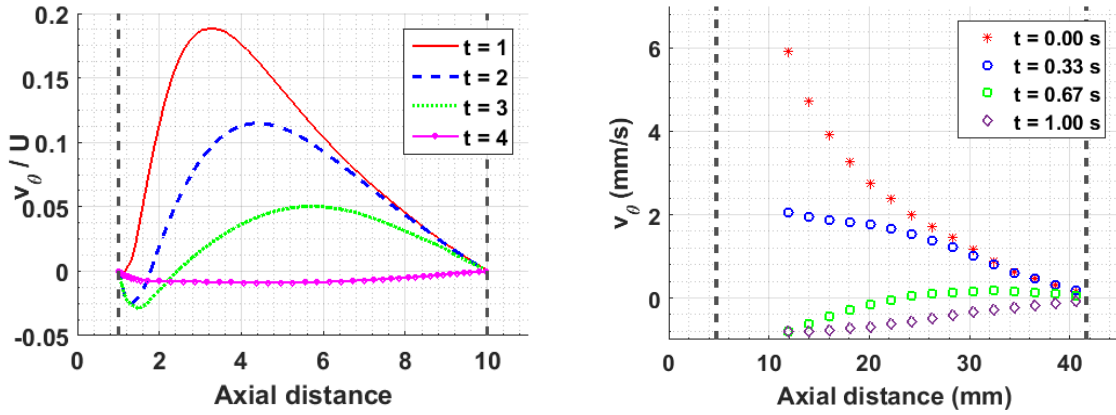


Figure 8. Azimuthal velocity as a function of r at the different times indicated in the legend box. In panel (a) corresponding to the numerical the simulation of the Oldroyd-B fluid the units of time are arbitrary. Panel (b) corresponds to experimental data for the P1G30 fluid.

the dependence of S with E , for $Re=0.1$ and different values of G . As can be seen from the figure, the overshoot exhibits almost a linear dependence with E for values above a characteristic value E_s , while for $E < E_s$ the overshoot values are very small. This behavior explains the large differences in the undershoot values obtained for the distinct fluid samples considered in the experiments.

In Fig. 8 we show the azimuthal velocity, v_θ , at different radial positions during the decay of the vortex flow after the inner cylinder abruptly stops. As it can be observed in this figure, the temporal evolution and spatial dependence of azimuthal velocity is very similar to those observed in the experiments. The velocity first changes sign near the inner cylinder and later the sign change propagates to larger radial positions.

As a consequence, it can be concluded that using the Oldroyd-B model is possible

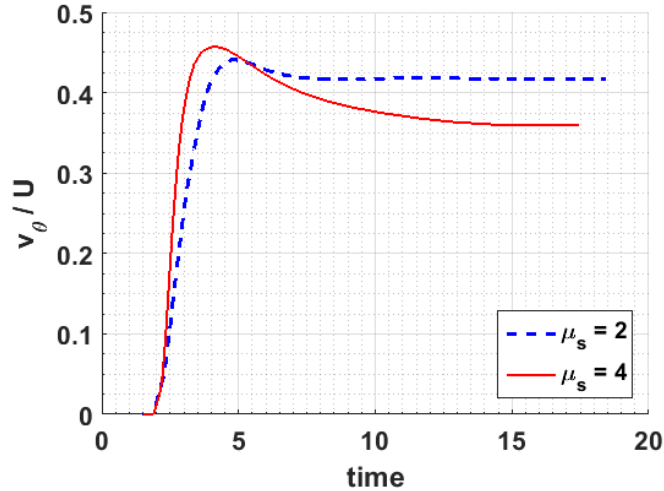


Figure 9. Effect of the solvent viscosity variation in a simulation of the Oldroyd-B model. The solid line corresponds to $De=0.5$, $Re = 0.025$ ($\mu_s = 4$) and the dashed line to $De=0.25$, $Re=0.05$ ($\mu_s = 2$).

to identify the roles of the elasticity component and solvent viscosity in the formation and decay of the vortex. It is worth noticing that in accordance with the experiments, the velocity profiles do not exhibit the oscillations that are present in the solutions of [5] for the fractional Oldroyd-B model. This fact is probably caused by the differences in the boundary conditions taken by these authors, while in [5] the vortex is unbounded, in our experiments and simulations the vortex flow is confined in a cylindrical region. Another remarkable aspect is that the Oldroyd-B model is not adequate to give account of the influence of the viscosity solvent μ_s on the evolution of the vortex. In this model, the reduction of μ_s at constant concentration m implies that the relaxation time λ and consequently De are decreased, although the parameter G remains unaltered. Such reduction of De at constant G always produces the decrease of the overshoot, as it is shown in Fig. 7. Thus the Oldroyd-B model cannot explain the increase of the overshoot due to the reduction of μ_s observed in the experiments. By comparing the overshoot in P1G60 and P1G30 reported in the experiments of Section 2, it can be seen that the last exhibited a larger overshoot than the former in spite of presenting a lower viscosity solvent. In order to study whether the shear thinning effects cause this kind of dependence, in the next section we introduce a model with strain dependent viscosity.

4.2. Shear-thinning effects

To study the influence of shear thinning effects on the evolution of the vortex flow, we used the White-Metzer (WM) constitutive model [19]. The considered governing equations are formally the same as Eqs. (1), but with a relaxation time that is a function of second invariant of the rate of deformation tensor \mathbf{D} , $\dot{\gamma} = 2\text{tr}(\mathbf{D}^2)$. Assuming that $\lambda(\dot{\gamma})$ obeys the Carreau expression, due to the relation $\mu_p = \lambda G$, it follows that the

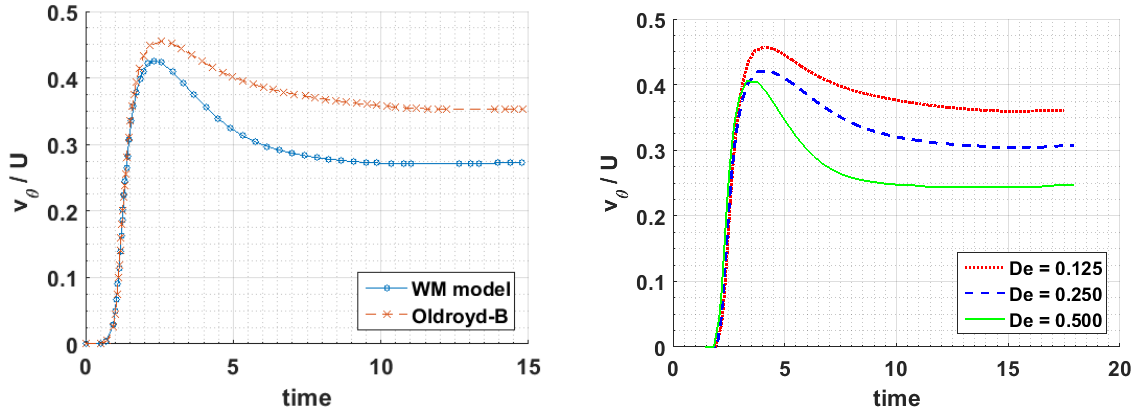


Figure 10. Shear-thinning effects on the overshoot. The temporal evolution of the azimuthal velocity at a fixed axial distance is plotted in panel (a) for the two models considered; Oldroyd-B (the overshoot results $M_p = 0.28$) and WM model ($M_p = 0.57$). Panel (b) illustrates the angular velocity dependence on the overshoot using the WM model. The Deborah number, $De = \lambda_0\Omega$ (indicated in the legend box) was varied by changing Ω and keeping λ_0 fixed. In both cases $E = 18$, $Re=0.1$ and the power index in the WM model was $n = 0.43$ (the value corresponding to P1G60 sample). The value of λ_0 used in the simulation of the WM model coincides with the one of λ used in the simulation of the Oldroyd-B model.

polymer viscosity is also described by the Carreau model. The resulting total viscosity $\mu = \mu_s + \mu_p$ is

$$\mu = \mu_s + \mu_{p0}[1 + (\lambda_0\dot{\gamma})^2]^{(n-1)/2} \quad (5)$$

where λ_0 and μ_{p0} are given by relations (3) and (4). Notice that when $\dot{\gamma} \rightarrow 0$, the constant viscosity of the Oldroyd-B model is recovered.

Figure 10 presents the curves of azimuthal velocity for the Oldroyd-B and WM models. The value of λ_0 used in the numerical simulations of the WM model coincides with the value of λ used in the simulations of the Oldroyd-B model and both of them were performed with the same value of Re . These curves show that the shear thinning effect favors the overshoot, which is reflected in the increment of the parameter M_p .

Another fact observed experimentally is that the stationary angular velocity of the inner cylinder clearly increases the overshoot. Figure 10(b) shows the azimuthal velocities for three different angular velocities according to the WM model. From these curves it can be observed that the angular velocity of the inner cylinder leads to an increment in the overshoot value. This result is coherent with the influence of the shear thinning on this quantity shown in panel (a). As the angular velocity is decreased, the strain $\dot{\gamma}$ also decreases and we recover the Oldroyd-B model which exhibits a smaller overshoot. On the opposite situation, when the angular velocity is increased, the shear-thinning effects are more notorious and the overshoot is enhanced.

The reported numerical results explain the effect of the variations in the solvent viscosity. In general, an increment in the solvent viscosity reduces the shear-thinning

effects. Due to this reason, to prepare a Boger fluid sample *i.e.* a fluid with elastic behavior but constant viscosity, a very high solvent viscosity is recommended [20, 21]. As a consequence, a reduction in the solvent viscosity increases the shear-thinning effects, which in turn increments the overshoot.

5. Conclusion

We studied the transient behaviour of viscoelastic vortex flows between concentric cylinders by means of experiments and numerical simulations. We study both the formation, that develops from the quiescent fluid when the inner cylinder suddenly begins to rotate and the decay, when the inner cylinder abruptly stops. In the experiments, digital particle velocimetry was employed to obtain the velocity fields in glycerin and polyacrylamide solutions while the numerical simulations were based on implementations of the Oldroyd-B and White-Metzer models using the commercial package COMSOL. For the parameter values considered here the flows exhibit axial symmetry.

We found that, in contrast with Newtonian flows in which the azimuthal velocity increases or decreases monotonically to a steady value, the non-Newtonian cases are characterized by positive or negative maximum values followed by the decay to a stationary value. As a way to characterize these transient effects we introduced non-dimensional parameters, overshoot and undershoot, similar to those well-known in control theory. The experimental results, supplemented with numerical simulations reveal that, although this phenomenon is ubiquitous in viscoelastic flows, their magnitude depend strongly on the distance to the rotation center, the angular velocity and also on the fluid characteristics. In particular, we showed that the overshoot and the undershoot depend on the elastic component and also on the solvent viscosity.

The simulations performed with the Oldroyd-B model with boundary conditions equivalent to experimental conditions reproduce very well the observed flows, showing that this model is able to capture qualitatively the phenomenon. In particular, the overshoot and undershoot shapes agree very well. The several inflexion points in the profile of the azimuthal velocity reported by Fetecau et al [5] were not observed suggesting that this disagreement is probably caused by the fact the boundary conditions are different. As a general observation the Oldroyd-B model can explain qualitatively some aspects of the behavior of the unsteady vortex, but to describe the dependence of the flow with the solvent viscosity and the velocities at the material boundaries a model including shear thinning effects is required.

As the Oldroyd-B model was not able to capture shear-thinning effects, we introduced the WM model. Performing numerical simulations performed with this model, we showed that the overshoot increment is produced by the reduction of the solvent viscosity and it is directly related to shear-thinning effects. The dependence of the overshoot with the angular velocity of the inner cylinder was also explained with the WM model. As a general result, the viscosity increase with the axial distance due

to the shear-thinning effect favors the overshoot. A similar argument can be proposed to explain the similarities and differences between the overshoot in Fig. 3 and the undershoot in Fig. 6. Both quantities grow with axial distance until reaching a plateau where the value remains constant. These increments with axial distance can be related to the decrements of shear stresses also with axial distance and explain that the undershoot reaches the stationary value closer to the center than in the case of the overshoot.

The experimental results reported in our experiments, in particular, the existence of the non-monotonic behavior of the azimuthal velocity illustrates a notable characteristic of viscoelastic flows that has previously received few attention. The academic and applied interest in the dynamics of viscoelastic fluids encourages further experimental and numerical investigations about this phenomenon.

Acknowledgements

We acknowledge financial support from grant Fisica Nolineal (ID 722) Programa Grupos I + D CSIC 2018 (UdelaR, Uruguay) and PEDECIBA (UdelaR, MEC, Uruguay).

References

- [1] F. Irgens, *Rheology and non-newtonian fluids*. Springer, 2014, vol. 190.
- [2] Y. L. Joo and E. S. Shaqfeh, “The effects of inertia on the viscoelastic dean and taylor–couette flow instabilities with application to coating flows,” *Physics of Fluids A: Fluid Dynamics*, vol. 4, no. 11, pp. 2415–2431, 1992.
- [3] E. S. Shaqfeh, “Purely elastic instabilities in viscometric flows,” *Annual Review of Fluid Mechanics*, vol. 28, no. 1, pp. 129–185, 1996.
- [4] H. Qi and H. Jin, “Unsteady rotating flows of a viscoelastic fluid with the fractional maxwell model between coaxial cylinders,” *Acta Mechanica Sinica*, vol. 22, no. 4, pp. 301–305, 2006.
- [5] C. Fetecau, C. Fetecau, M. Khan, and D. Vieru, “Decay of a potential vortex in a generalized oldroyd-b fluid,” *Applied mathematics and computation*, vol. 205, no. 1, pp. 497–506, 2008.
- [6] M. Khan, S. H. Ali, C. Fetecau, and H. Qi, “Decay of potential vortex for a viscoelastic fluid with fractional maxwell model,” *Applied Mathematical Modelling*, vol. 33, no. 5, pp. 2526–2533, 2009.
- [7] C. T. Hill, “Nearly viscometric flow of viscoelastic fluids in the disk and cylinder system. ii: Experimental,” *Transactions of the Society of Rheology*, vol. 16, no. 2, pp. 213–245, 1972.
- [8] C. Day, J. A. Harris, J. Soria, D. Boger, and M. Welsh, “Behavior of an elastic fluid in cylindrical swirling flow,” *Experimental thermal and fluid science*, vol. 12, no. 2, pp. 250–255, 1996.
- [9] M. Escudier and L. Cullen, “Flow of a shear-thinning liquid in a cylindrical container with a rotating end wall,” *Experimental thermal and fluid science*, vol. 12, no. 4, pp. 381–387, 1996.
- [10] S. Tamano, M. Itoh, Y. Ide, and K. Yokota, “Vortex shedding in confined swirling flow of polymer solutions,” *Physics of Fluids*, vol. 19, no. 2, p. 023103, 2007.
- [11] A. Groisman and V. Steinberg, “Couette-taylor flow in a dilute polymer solution,” *Physical Review Letters*, vol. 77, no. 8, p. 1480, 1996.
- [12] B. Martínez-Arias and J. Peixinho, “Torque in taylor–couette flow of viscoelastic polymer solutions,” *Journal of Non-Newtonian Fluid Mechanics*, vol. 247, pp. 221–228, 2017.
- [13] O. Katsuhiko, *Modern control engineering*, 2010.
- [14] J. G. Oldroyd, “On the formulation of rheological equations of state,” *Proceedings of the Royal Society of London. Series A. Mathematical and Physical Sciences*, vol. 200, no. 1063, pp. 523–541, 1950.

- [15] R. G. Larson, *Constitutive equations for polymer melts and solutions: Butterworths series in chemical engineering*. Butterworth-Heinemann, 2013.
- [16] COMSOL Inc. COMSOL Multiphysics®. [Online]. Available: <https://www.comsol.com/model/flow-of-viscoelastic-fluid-past-a-cylinder-4383>
- [17] J. M. Martel and M. Toner, “Inertial focusing dynamics in spiral microchannels,” *physics of fluids*, vol. 24, no. 3, p. 032001, 2012.
- [18] L. Zhu, E. Lauga, and L. Brandt, “Self-propulsion in viscoelastic fluids: Pushers vs. pullers,” *Physics of fluids*, vol. 24, no. 5, p. 051902, 2012.
- [19] J. L. White, “Dynamics of viscoelastic fluids, melt fracture, and the rheology of fiber spinning,” *Journal of Applied Polymer Science*, vol. 8, no. 5, pp. 2339–2357, 1964.
- [20] E. Bot, M. Hulsen, and B. Van den Brule, “The motion of two spheres falling along their line of centres in a boger fluid,” *Journal of non-newtonian fluid mechanics*, vol. 79, no. 2-3, pp. 191–212, 1998.
- [21] D. Freire, L. Sarasúa, A. Vernet, S. Varela, G. Usera, C. Cabeza, and A. Martí, “Separation regimes of two spheres falling in shear-thinning viscoelastic fluids,” *Physical Review Fluids*, vol. 4, no. 2, p. 023302, 2019.